Applied Physics A (2023) 129:538
https://doi.org/10.1007/s00339-023-06807-7

Applied Physics A
Materials Science & Processing

Temperature-dependent current–voltage characteristics of *p*-$GaSe_{0.75}S_{0.25}$/*n*-Si heterojunction

M. Isik[1] · O. Surucu[1] · N. M. Gasanly[2,3]

Received: 24 April 2023 / Accepted: 22 June 2023 / Published online: 4 July 2023

Abstract
$GaSe_{0.75}S_{0.25}$ having layered structure is a potential semiconductor compound for optoelectronics and two-dimensional materials technologies. Optical and structural measurements of the $GaSe_{0.75}S_{0.25}$ thin film grown on the glass substrate showed that the compound has hexagonal structure and band energy of 2.34 eV. $GaSe_{0.75}S_{0.25}$ thin film was also grown on the silicon wafer and *p*-$GaSe_{0.75}S_{0.25}$/*n*-Si heterojunction was obtained. To make the electrical characterization of this diode, temperature-dependent current–voltage (*I*–*V*) measurements were carried out between 240 and 360 K. Room temperature ideality factor and barrier height of the device were determined from the analyses of *I*–*V* plot as 1.90 and 0.87 eV, respectively. Temperature-dependent plots of these electrical parameters showed that the ideality factor decreases from 2.19 to 1.77, while barrier height increases to 0.94 from 0.71 eV when the temperature was increased from 240 to 360 K. The conduction mechanism in the heterojunction was studied considering the Gaussian distribution due to presence of inhomogeneity in barrier height. The analyses presented the mean zero-bias barrier height, zero-bias standard deviation, and Richardson constant.

Keywords Schottky diode · Optoelectronics · Solar cell · GaSe · GaS

1 Introduction

GaSe and GaS compounds are two materials that have an effective position in especially optoelectronic applications [1–3]. The fact that these compounds have a layered structure has also put themselves an important place in the field of two-dimensional material technology [4]. Both compounds crystallize in the hexagonal structure, and the lattice parameters were found to be $a = 0.375$ nm, $c = 1.595$ nm for GaSe and $a = 0.3578$ nm, $c = 1.547$ nm for GaS [5]. Studies on GaSe having direct band energy of 1.9 eV have shown the usability of this compound in photovoltaic, laser, optoelectronic, photocatalytic and thermoelectric applications [6–8]. GaS compound, which has a greater band energy (~ 2.6 eV) than GaSe, has been shown in the literature to have effective properties for optoelectronic applications [9, 10]. The ability to make these two compounds, which have weak bonds between layers, two-dimensional, make these compounds important research topics in the field of 2D device technologies.

As a result of the replacement of the Se atoms in the GaSe compound with the S atoms, $GaSe_xS_{1-x}$ ternary semiconductor compounds are formed. Se–S displacement allows the structural and optical properties of ternary compounds to be adjusted depending on the composition [11, 12]. The studies on $GaSe_xS_{1-x}$ compounds have revealed that the band energy and lattice parameter tune almost linearly with composition. This tuning behavior has very important benefits, especially for optoelectronic applications. $GaSe_{0.75}S_{0.25}$ compound is formed by replacing 25% of the Se atoms in the GaSe compound with S atoms. Detailed structural and optical examination of the single crystal form of the compound has been revealed by previous studies in the literature [13, 14]. In our previous study, the thin film form of the compound was grown, and the necessary characterizations were made [15]. The bandgap energy of the $GaSe_{0.75}S_{0.25}$ thin film was found as 2.21 eV which provides the compound a potential in visible light optoelectronic applications. Our aim in the present study is to make Si-based $GaSe_{0.75}S_{0.25}$ Schottky

✉ M. Isik
mehmet.isik@atilim.edu.tr

[1] Department of Electrical and Electronics Engineering, Atilim University, 06836 Ankara, Turkey

[2] Department of Physics, Middle East Technical University, 06800 Ankara, Turkey

[3] Virtual International Scientific Research Centre, Baku State University, 1148 Baku, Azerbaijan

diode and to accomplish the electrical characterization of this construction. The various heterostructures formed from GaSe and GaS compounds have been previously reported. Au/GaSe:Ce [16], Au/GaSe:Nd [17], GaSe/$MoSe_2$ [18], Al/GaSe/In [19], GaS:WS_2 [20] and graphene/GaS [21] are some of the heterostructures formed for various technological applications. In the literature, there is a heterostructure of MgO/$GaSe_{0.75}S_{0.25}$ obtained with the compound we want to study [22, 23]. It was reported from the detailed electrical characterizations that MgO/$GaSe_{0.75}S_{0.25}$ heterostructure is a potential candidate for optoelectronic devices. In the present work, *p*-$GaSe_{0.75}S_{0.25}$/*n*-Si structure was formed for the first time by thermal evaporation method. The device behavior and diode parameters were determined from the temperature dependent current–voltage (*I–V*) characteristics. The variation of ideality factor and barrier height with temperature was investigated considering Gauss distribution in barrier height and mean zero-bias barrier height, zero-bias standard deviation, and Richardson constant were determined from the analyzed.

2 Experimental details

Single crystal of $GaSe_{0.75}S_{0.25}$ was obtained using the Bridgman method. The growth details and basic structural properties of the produced single crystals were reported in our previous studies [11, 14]. Single crystal was brought into powder form and thin film growth was performed by thermal evaporation method. Before deposition of thin films on *n*-Si wafer, the following chemical cleaning method was applied: to remove any organic contaminants or residues, the *n*-Si wafer was first rinsed with acetone. To further remove organic impurities, n-Si wafers were rinsed with isopropyl alcohol after rinsing with acetone. Then, the n-Si wafer was dried using clean, dry nitrogen gas. Deposition process on glass and Si-wafer substrates were carried out as follows: the $GaSe_{0.75}S_{0.25}$ powder was placed into a tungsten boat filament. The substrates were placed about 25 cm above the evaporation source. The substrates were rotated during the growth process to get a uniform thin film. The deposition rate of ~ 1–2 Å/s was monitored using Inficon XTM/2 quartz crystal monitor. Dektak 6 M thickness profilometer presented the thickness of the growth films around 500 nm. The thin films were annealed at 300 °C for 30 min. under nitrogen atmosphere.

X-ray diffraction (XRD) experiment was performed using Rigaku miniflex diffractometer with CuKα radiation ($\lambda = 0.154049$ nm). SEM experiments were performed by ZEISS EVO 15-SEM to present surface morphology of the deposited structures. Transmission measurement was carried out by Jenway 6400 model spectrophotometer. Due to ohmic contact behavior, the back contact of the Schottky diode was deposited on Si-wafer by thermal evaporation of silver (Ag) metal, while the front contact was deposited on $GaSe_{0.75}S_{0.25}$ thin film by indium (In) metal (see Fig. 1). To improve the quality of the contacts, after the deposition of contacts was made, the annealing processes were done at 100 and 300 °C for 30 min under nitrogen atmosphere for Ag and In contacts, respectively. The resistivity and dopant concentration of the used Si-wafer were 2.5 Ω.cm and 1.87×10^{15} cm^{-3}, respectively. This annealing temperature was applied, since we saw that the best ohmic contact was observed at 100 °C when we annealed at different temperatures. Temperature-dependent current–voltage measurements were applied using Keithley 2401 model source meter, LakeShore DSC-91 C temperature controller and Model 22 CTI Cryogenics closed-cycle helium cryostat.

3 Results and discussion

XRD pattern of $GaSe_{0.75}S_{0.25}$ thin film, which was grown on glass substrate by thermal evaporation method, is shown in Fig. 2. As a result of measurements performed in the range of 20–60°, three well-defined peaks were observed around 22.50°, 28.05° and 49.25°. The presence of these peaks primarily indicates that the deposited thin-film compound has a good crystalline structure. The observed peaks are consistent with the peaks observed in the XRD patterns of GaSe and $GaSe_{0.75}S_{0.25}$ compounds [15, 24]. The peaks observed in the thin film $GaSe_{0.75}S_{0.25}$ were associated with the planes (004), (100) and (110) of the hexagonal crystal structure considering the results of detailed structural studies of $GaSe_{1-x}S_x$ compounds [25]. Figure 3 indicates the SEM images of the deposited $GaSe_{0.75}S_{0.25}$ thin film on glass substrate and *p*-$GaSe_{0.75}S_{0.25}$/*n*-Si heterojunction. According to given SEM images, it is seen that the film surface is uniform and smooth.

Transmission measurements were performed to obtain the band energy of $GaSe_{0.75}S_{0.25}$ thin film grown on glass substrate. The absorption coefficient (α) was calculated using the relation $\alpha = -\ln(T)/d$, where T is the transmittance and

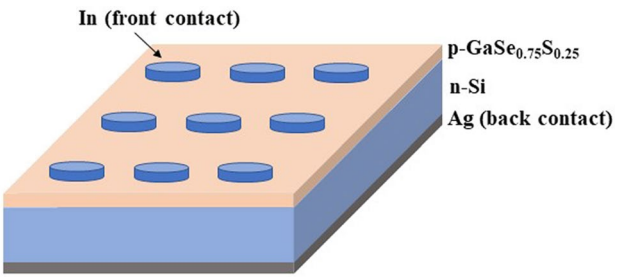

Fig. 1 Schematic cross section of the In/*p*-$GaSe_{0.75}S_{0.25}$/*n*-Si/Ag diode structure

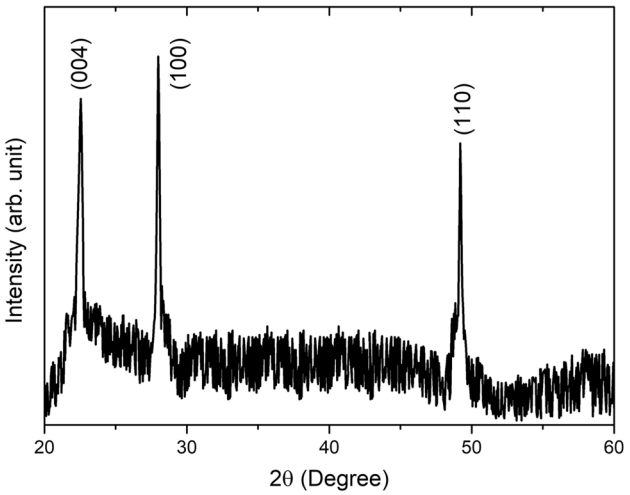

Fig. 2 XRD pattern of $GaSe_{0.75}S_{0.25}$ thin film

$d = 500$ nm is the thickness of the film. The absorption spectrum obtained using the transmission data was drawn in the range of 380–750 nm, as shown in Fig. 4. The absorption coefficient (α) and bandgap energy (E_g) are related to each other as follows [26]:

$$(\alpha h\nu) = A\left(h\nu - E_g\right)^n \tag{1}$$

where A is photon energy ($h\nu$) independent constant and n is parameter describing characteristics of the bandgap. When Eq. (1) is rearranged using mathematical operations, the following expression is obtained [26]:

$$\frac{d(ln(\alpha h\nu))}{d(h\nu)} = \frac{n}{h\nu - E_g} \tag{2}$$

This expression is used to get bandgap energy of the thin film. For this purpose, the $dln(\alpha h\nu)/d(h\nu)$ vs. $h\nu$ plot was drawn, as shown in the Fig. 4. The energy value at which the observed peak reaches its maximum value in this plot corresponds to the bandgap energy. As shown in Fig. 4, inset, it reaches its peak maximum value of 2.34 eV. Optical studies on $GaSe_{1-x}S_x$ crystals indicated the band energy for crystal of composition $x = 0.25$ as 2.13 eV [11] and 2.17 eV [25]. The band energy we found for the $GaSe_{0.75}S_{0.25}$ thin film is about 0.2 eV larger than these reported values. It is well-known that as the thickness decreases, the band energy increases due to quantum confinement effect [27]. Therefore, it is reasonable that the band energy of the thin film is 2.34 eV more than the band energy of the crystal. The 2.34 eV energy found corresponds to the visible region and, therefore, indicates that the $GaSe_{0.75}S_{0.25}$ thin film is a potential candidate for optoelectronic devices.

The compound was deposited on n-Si wafer to investigate the diode characteristics of the $GaSe_{0.75}S_{0.25}$ thin film. Temperature-dependent current–voltage measurements of p-$GaSe_{0.75}S_{0.25}$/n-Si were performed to examine diode behavior and obtain the relevant diode parameters. Figure 5 shows the I–V graph of In/p-$GaSe_{0.75}S_{0.25}$/n-Si structure for the forward bias zone at room temperature. Inset of the figure indicates the I–V plot for In/$GaSe_{0.75}S_{0.25}$/In structure. As seen from this plot, I–V characteristics for In/$GaSe_{0.75}S_{0.25}$/In structure is linear indicating the presence of ohmic behavior, while non-linear behavior was observed for In/p-$GaSe_{0.75}S_{0.25}$/n-Si electrodes. The $GaSe_{0.75}S_{0.25}$ compound is structurally and optically close to GaSe. Similar ohmic behavior was also in the literature on the In/GaSe/In heterostructure [17, 28].

Figure 6 shows the temperature-dependent I–V graphs of In/p-$GaSe_{0.75}S_{0.25}$/n-Si structure for the forward bias zone. As can be seen from the inset plot, heterostructure exhibited a rectifier behavior and I–V plot presented exponential behavior at positive bias region. The rectification ratio at applied temperatures for applied bias voltage of ± 1.0 V

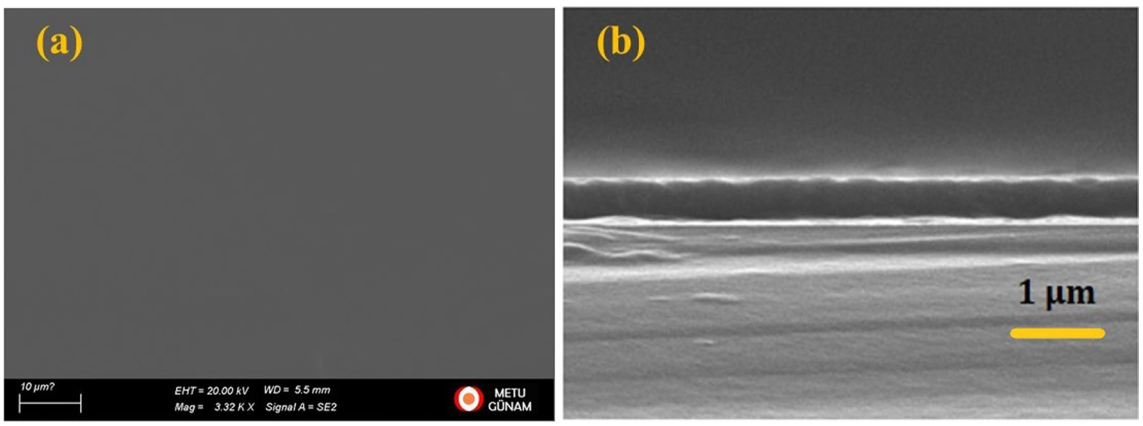

Fig. 3 (**a**) SEM image of the $GaSe_{0.75}S_{0.25}$ thin film deposited on glass substrate and (**b**) cross-sectional SEM image view of the p-$GaSe_{0.75}S_{0.25}$/n-Si heterojunction

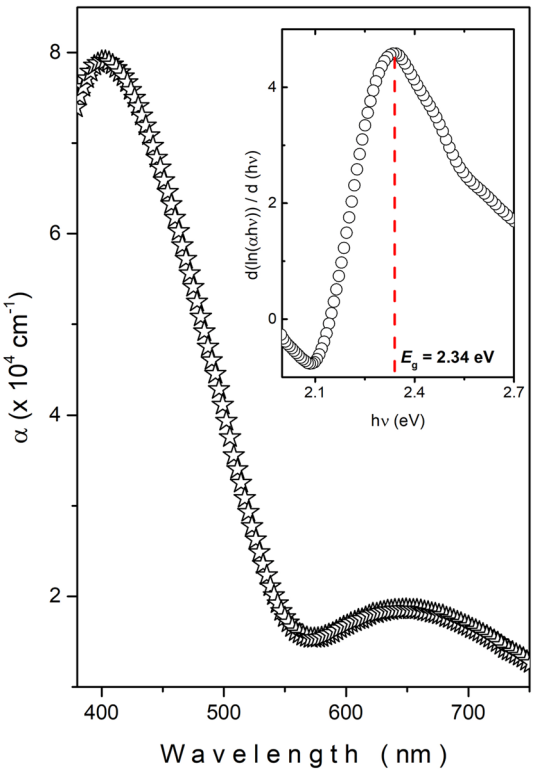

Fig. 4 Spectrum of absorption coefficient. Inset indicates the $d\ln(\alpha h\nu)/d(h\nu)$ vs. $h\nu$ plot

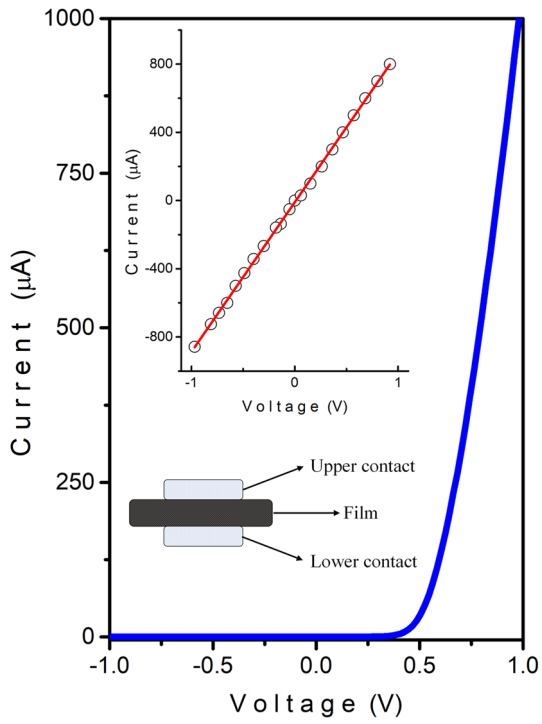

Fig. 5 *I–V* plots for positive bias voltage at room temperature for In/$GaSe_{0.75}S_{0.25}$/Si heterojunction. Inset indicates the *I–V* plot for In/$GaSe_{0.75}S_{0.25}$/In

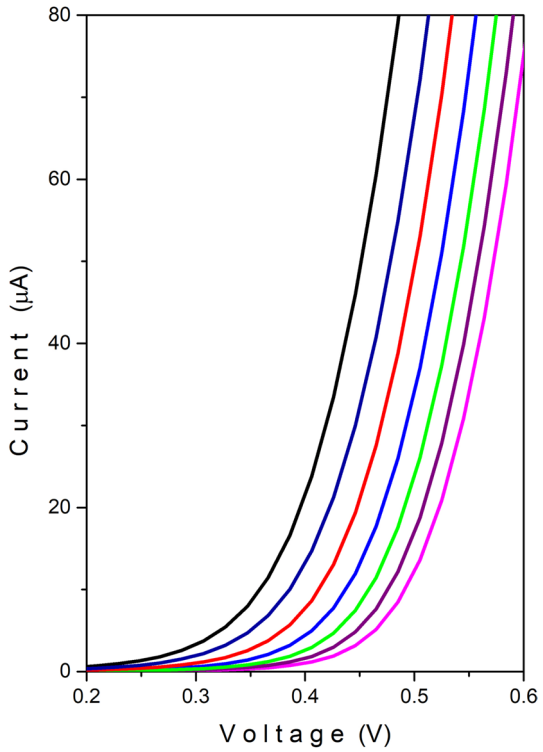

Fig. 6 *I–V* plots for positive bias voltage at various temperatures

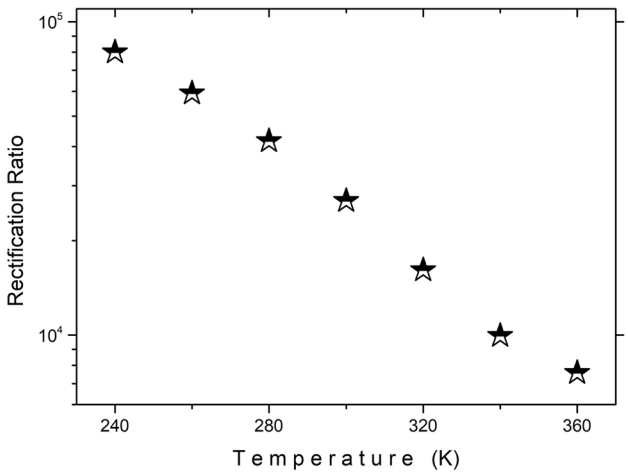

Fig. 7 Temperature dependence of rectification ratio of *p*-$GaSe_{0.75}S_{0.25}$/*n*-Si heterojunction

was calculated using the expression of $I_{forward}/I_{reverse}$. Figure 7 indicates the temperature-dependent plot of rectification ratio which decreased from 8.0×10^4 to 7.6×10^3 as the temperature increased from 240 to 360 K. The temperature–rectification ratio behavior is well-consistent with previously reported results [29, 30]. The decrease of rectification ratio with increasing temperature is associated with several reasons, such as barrier height lowering, increased

carrier generation, increased carrier mobility and impact on metal–semiconductor interface.

The theory of thermionic emission is often used instead of diffusion theory in heterostructures to explain the current flowing through the junction. The reason of this point is the fact that band alignment at heterojunctions produces a barrier that inhibits the diffusion of charge carriers and makes the thermionic emission dominant mechanism for current transport. According to thermionic emission theory, forward current (I) is expressed as follows [31]:

$$I = I_0\left[exp\left(\frac{q(V - IR_s)}{nkT}\right) - 1\right] \tag{3}$$

where I_0 is the reverse saturation current, q is the electronic charge, V is the applied bias voltage, R_s is the series resistance, n is the diode ideality factor, k is the Boltzmann constant, T is the absolute temperature. The reverse saturation current is described as follows [31]:

$$I_0 = AA^*T^2\left[exp\left(-\frac{q\Phi_{b0}}{kT}\right)\right] \tag{4}$$

where A is the effective diode area, A^* is the Richardson constant (112 A/(cm^2 K^2) for n-Si [32]), Φ_{b0} is the zero bias barrier height. The ideality factor and reverse saturation current are determined by plotting ln(I)-V plot in the linear region and by applying linear fit to the plot. The ideality factor is given by the following expression:

$$n = \frac{q}{kT}\left(\frac{dV}{dln(I)}\right) \tag{5}$$

The ln(I)-V plots of the experimental data are given in Fig. 8. As a result of the linear fit application and using Eqs. (4) and (5), the electrical parameters of the room temperature data were found as $I_0 = 1.29 \times 10^{-9}$ A, $n = 1.90$ and $\Phi_{b0} = 0.87$ eV. In an ideal heterojunction diode, the n value is equal to 1. However, in real diodes, the presence of various factors such as serial resistance, inhomogeneities in barrier height, carrier recombination causes a deviation from ideal diode equation. The ideality factor is, therefore, usually between 1 and 2 in most heterojunction diodes. The value of 1.90 that we obtain is also included in this range.

The barrier height and ideal factor were determined for all applied temperatures applied as mentioned above. The temperature-dependent variation of these two electrical parameters is shown in Fig. 9. As can be seen from the figure, while the barrier height increased as the temperature increased, the ideal factor exhibited a decreasing behavior with increase in temperature. Similar variation in barrier height and ideal factor with temperature have been observed in many articles in the literature [33–35]. The fact that the barrier height (ideal factor) decreases (increases) with increase of temperature is

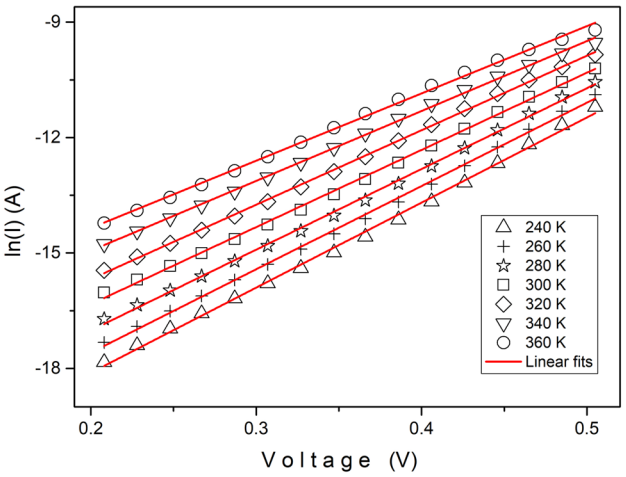

Fig. 8 ln(I)-V plots for the linear region

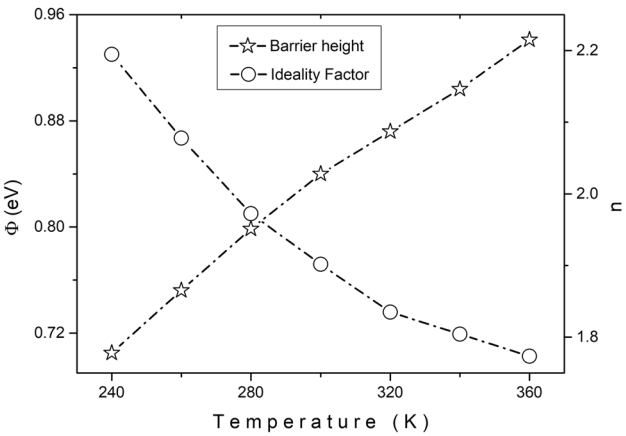

Fig. 9 Temperature dependencies of barrier height and ideality factor

explained by the inhomogeneity in the barrier height in the diode [36]. The fact that the value n is greater than the ideal value of 1 is also a point that supports inhomogeneity. The fact that the ideal factor approaches to 1 at the applied low temperature values and also that the rectification ratio (see Fig. 7) is high at low temperatures shows that the designed p-$GaSe_{0.75}S_{0.25}$/n-Si heterojunction diode is closer to the ideal behavior at the low temperatures.

Figure 10 shows the dependence of the barrier height to the ideal factor. As can be seen from the graph, an approximately linear relationship is seen between these parameters. The inverse relationship between barrier height and the ideal factor is explained as follows [31]: The decrease in barrier height in the diodes leads to an increased probability of tunneling charge carriers. This increase leads to an increase in leakage current and a decrease in the rectification ratio of the diode. As a result of this situation, the

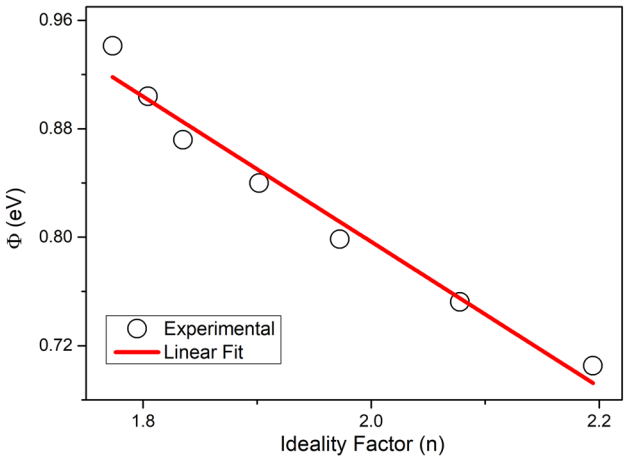

Fig. 10 Barrier height vs. ideality factor plot

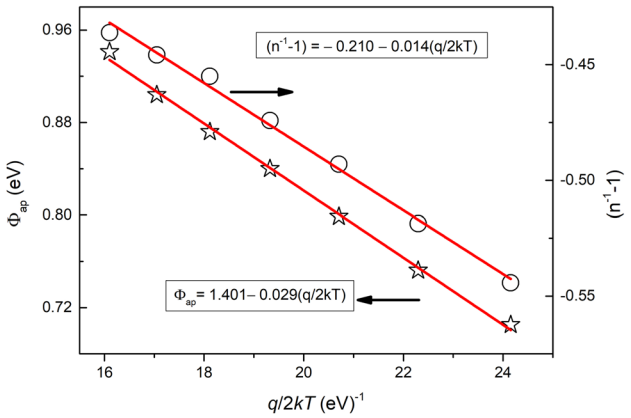

Fig. 11 Dependencies of Φ_{ap} and $(n^{-1}-1)$ on $q/2kT$. Solid lines represent linear fits

ideal factor increases. When the barrier height increases, the change in the specified processes is exactly the opposite. That is, the tunneling probability decreases, so the leakage current decreases, and the ideal factor decreases.

The thermionic emission theory is based on homogeneous barrier height of the diode. For the inhomogeneous diodes, Gaussian distribution of barrier height studies were accomplished. As a result of the analysis based on the Gaussian distribution, the barrier height obtained experimentally was expressed as follows [36, 37]:

$$\Phi_{ap} = \overline{\Phi}_{B0} - \frac{q\sigma_0^2}{2kT} \tag{6}$$

where $\overline{\Phi}_{B0}$ and σ_0 are the mean Schottky barrier height and its standard deviation at zero-bias, respectively. According to Eq. (6), the plot of Φ_{ap} vs. $q/2kT$ shows a linear behavior whose slope and its intercept give the σ_0 and $\overline{\Phi}_{B0}$, respectively. Figure 11 indicates the corresponding plot and applied linear fit which presented the electrical parameters as $\overline{\Phi}_{B0} =$ 1.401 eV and $\sigma_0 = 0.17$. The experimentally obtained apparent ideality factor (n_{ap}) is given in the Gaussian distribution model by the following expression [36, 37]:

$$\left(\frac{1}{n_{ap}} - 1\right) = -\rho_2 + \frac{q\rho_3}{2kT} \tag{7}$$

where the coefficient of ρ_2 and ρ_3 indicates the voltage deformation of the Gauss distribution of the barrier height. According to Eq. (7), plot of $(n_{ap}^{-1} - 1)$ vs. $q/2kT$ exhibits a linear dependence from which ρ_2 and ρ_3 can be obtained. Figure 11 shows the mentioned plot and linear fitted line which indicated the parameters as $\rho_2 = 0.210$ and $\rho_3 = 0.014$.

The mean barrier height ($\overline{\Phi}_{b0}$) and Richardson's constant (A^*) can be calculated using the following equation for the Gaussian distribution of barrier height [36, 37]:

$$ln\left(\frac{I_0}{T^2}\right) - \left(\frac{q^2\sigma_0^2}{2k^2T^2}\right) = ln(AA^*) - \frac{q\overline{\Phi}_{b0}}{kT} \tag{8}$$

Using the determined values for experimentally and then plotting $\ln(I_0/T^2) - (q^2\sigma_0^2/2k^2T^2)$ vs. q/kT, one can obtain the $\overline{\Phi}_{b0}$ and A^* values from the slope and intersection point of the linear fitted line, respectively. Figure 12 shows the corresponding plot and applied linear fitted line which revealed the barrier height and Richardson's constant as $\overline{\Phi}_{b0} = 1.400$ eV and $A^* = 124$ A/(cm^{2}K^2). The obtained Richardson constant from this analysis is well-consistent with theoretical value of 112 A/(cm^2 K^2) for n-Si.

A schematic energy band diagram of the heterostructure by considering the bandgap energy and electron affinity values of the p-$GaSe_{0.75}S_{0.25}$ and n-Si materials

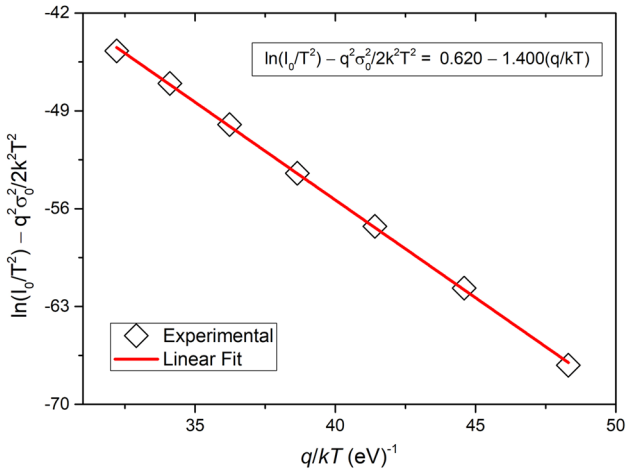

Fig. 12 Plot of $\ln(I_0/T^2) - (q^2\sigma_0^2/2k^2T^2)$ vs. q/kT for p-$GaSe_{0.75}S_{0.25}$/n-Si heterojunction diode. Solid line represents linear fit

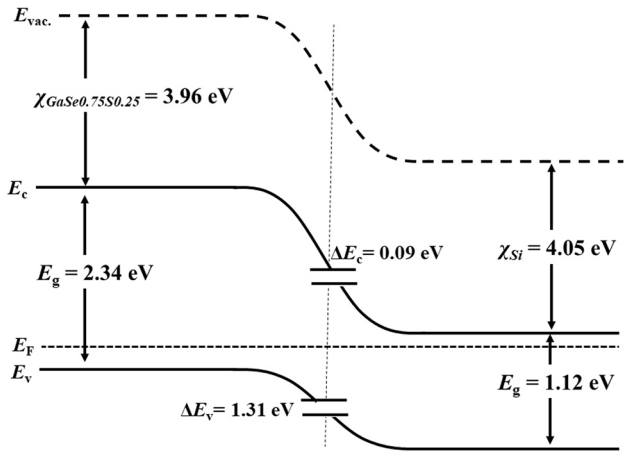

Fig. 13 Energy band diagram of p-$GaSe_{0.75}S_{0.25}$/n-Si heterojunction diode

is plotted as shown in Fig. 13. The E_g and χ values for p-$GaSe_{0.75}S_{0.25}$ and n-Si are E_g ($GaSe_{0.75}S_{0.25}$) = 2.34 eV, χ ($GaSe_{0.75}S_{0.25}$) = 3.96 eV [22], E_g (n-Si) = 1.12 eV, χ (n-Si) = 4.05 eV. The conduction band offset and valence band offset are expressed as follows [38]:

$$\Delta E_c = \chi_{Si} - \chi_{GaSe0.75S0.25} and \Delta E_v = E_{g,GaSe0.75S0.25} - E_{g,Si} + \Delta E_c \quad (9)$$

Using the corresponding energy values in Eq. (9), the ΔE_c and ΔE_v values were calculated as 0.09 and 1.31 eV, respectively. The higher ΔE_v than ΔE_c value indicates that electron injection from n-Si to p-$GaSe_{0.75}S_{0.25}$ is easier than hole injection from p-$GaSe_{0.75}S_{0.25}$ to n-Si. This dominant type of conduction in heterostructures results in large photocurrent [38, 39].

4 Conclusion

In the present work, temperature-dependent current–voltage characteristics of p-$GaSe_{0.75}S_{0.25}$/n-Si heterojunction diode were investigated. XRD pattern of the $GaSe_{0.75}S_{0.25}$ thin film deposited on glass substrate presented three well-defined diffraction peaks associated with hexagonal crystalline structure. The analysis of the absorption spectrum revealed the bandgap energy of the film as 2.34 eV. The analyses of the I–V plot of the device presented the ideality factor and barrier height as 1.90 and 0.87 eV, respectively. Temperature dependent measurements in the 240–360 K indicated that barrier height decreases, and ideality factor increases with increase of the temperature. This temperature-dependent behavior and the fact that the ideal factor is greater than one showed that the barrier height is not homogeneously distributed. The analyses based on Gaussian distribution of barrier height were used to get various electrical parameters. The mean barrier height, its standard deviation at zero-bias and Richardson constant were revealed as 1.400 eV, 0.17 and 124 A/(cm^2K^2), respectively.

Data availability Data are available uppon reasonable request.

References

1. L.R. Zeng, S.Y. Zhang, L.W. Yao, Z.S. Bi, Y.N. Zhang, P. Kang, J.F. Yan, Z.Y. Zhang, J.N. Yun, A type-II NGyne/GaSe heterostructure with high carrier mobility and tunable electronic properties for photovoltaic application. Nanotechnology **34**, 065702 (2023)
2. Q.Q. Luo, S.Q. Yin, Y.A. Tang, Z. Feng, X.Q. Dai, Two-dimensional GaS/$MoTe_2$ van der Waals heterostructures with tunable electronic and optical properties. Mat. Sci. Semicon. Proc. **152**, 107103 (2022)
3. M. Aitzhanov, N. Guseinov, R. Nemkayeva, Y. Sagidolda, Z. Tolepov, O. Prikhodko, Y. Mukhametkarimov, Growth and liquid-phase exfoliation of $GaSe_{1-x}S_x$ crystals. Materials **15**, 7080 (2022)
4. D. Barragan-Yani, J.M. Polfus, L. Wirtz, Native defects in monolayer GaS and GaSe: electrical properties and thermodynamic stability. Phys. Rev. Mater. **6**, 114002 (2022)
5. M. Isik, N. Gasanly, Ellipsometric study of optical properties of GaS_xSe_{1-x} layered mixed crystals. Opt. Mater. **54**, 155–159 (2016)
6. W.Y. Jiao, R. Hu, H.M. Yuan, S.H. Han, M.K. Li, Q.H. Tang, W. Lei, H.J. Liu, $HfSe_2$/GaSe heterostructure as a promising near-room-temperature thermoelectric material. J. Phys. Chem. C **126**, 20326–20331 (2022)
7. Z.H. Zhu, C.X. Zhang, M.S. Zhou, C.Y. He, J. Li, T. Ouyang, C. Tang, J.X. Zhong, Highly efficient water splitting in step-scheme PtS_2/GaSe van der Waals heterojunction. J. Appl. Phys. **132**, 055001 (2022)
8. T. Demirtas, C. Odaci, U. Aydemir, Enhanced photoresponse of PVP:GaSe nanocomposite thin film based photodetectors. Nanotechnology **33**, 205506 (2022)
9. S. Ahmed, J.P. Qiao, P.K. Cheng, A.M. Saleque, M.N.A. Ivan, T.I. Alam, Y.H. Tsang, Two-dimensional gallium sulfide as a novel saturable absorber for broadband ultrafast photonics applications. ACS Appl. Mater. Inter. **13**, 61518–61527 (2022)
10. M. Mosaferi, I.A. Sarsari, M. Alaei, Band structure engineering in gallium sulfide nanostructures. Appl. Phys. A **127**, 123 (2021)
11. M. Isik, N. Gasanly, Composition-tuned band gap energy and refractive index in GaS_xSe_{1-x} layered mixed crystals. Mater. Chem. Phys. **190**, 74–78 (2017)
12. A. Karatay, Controlling of two photon absorption properties by altering composition ratio of GaS_xSe_{1-x} crystals. Opt. Laser Technol. **111**, 6–10 (2019)
13. A.F. Qasrawi, N.M. Gasanly, Determination of carrier effective mass, impurity energy levels, and compensation ratio in Ga_4Se_3S layered crystals by Hall effect measurements. Phys. Stat. Sol. A **205**, 1662–1665 (2008)
14. M. Isik, N. Gasanly, Determination of optical constants and temperature dependent band gap energy of $GaS_{0.25}Se_{0.75}$ single crystals. J. Optoelectron. Adv. Mater. **19**, 374–378 (2017)
15. M. Isik, C. Emir, N.M. Gasanly, Structural and optical properties of thermally evaporated (GaSe)0.75-(GaS)0.25 thin films. Optik **230**, 166344 (2021)
16. H. Ertap, H. Kacus, S. Aydogan, M. Karabulut, Analysis of temperature dependent electrical characteristics of Au/GaSe Schottky

barrier diode improved by Ce-doping. Sensor Actuat. A-Phys. **315**, 112264 (2020)
17. H. Ertap, H. Kacus, S. Aydogan, M. Karabulut, Current-transport mechanisms in the Au/GaSe: Nd Schottky contact. J. Mater. Sci. Mater. El. **31**, 5198–5204 (2020)
18. J. Ning, Y. Zhou, J.C. Zhang, W. Lu, J.G. Dong, C.C. Yan, D. Wang, X. Shen, X. Feng, H. Zhou, Y. Hao, Self-driven photodetector based on a GaSe/$MoSe_2$ selenide van der Waals heterojunction with the hybrid contact. Appl. Phys. Lett. **117**, 163104 (2020)
19. H. Budak, S. Deman, F.S. Kaya, A. Ashkhasi, B. Gurbulak, Effect of temperature and illumination on the current-voltage characteristics of a Al/p-GaSe/In diode. J. Electron. Mater. **49**, 5698–5704 (2020)
20. Y. Lu, T.X. Chen, N. Mkhize, R.J. Chang, Y.W. Sheng, P. Holdway, H. Bhaskaran, J.H. Warner, GaS:WS_2 heterojunctions for ultrathin two-dimensional photodetectors with large linear dynamic range across broad wavelengths. ACS Nano **15**, 19570–19580 (2021)
21. K.D. Pham, H. Vu-Quang, C.V. Nguyen, Modulation of electronic properties and Schottky barrier in the graphene/GaS heterostructure by electric gating. Physica B **555**, 69–73 (2019)
22. A.F. Qasrawi, M.M. Abd-Alrazq, N.M. Gasanly, Optical dynamics of MgO/Ga_4Se_3S interface. J. Alloy. Compnd. **583**, 180–185 (2014)
23. A.F. Qasrawi, N.M. Gasanly, Energy band diagram and current transport mechanism in p-MgO/n-Ga_4Se_3S. IEEE T. Electron. Dev. **62**, 102–106 (2015)
24. H. Ertap, M. Yuksek, A. Karatay, A. Elmali, M. Karabulut, Linear and nonlinear absorption, SHG and photobleaching behaviors of Dy doped GaSe single crystal. Chin. J. Phys. **59**, 465–472 (2019)
25. C.H. Ho, C.C. Wu, Z.H. Cheng, Crystal structure and electronic structure of $GaSe_{1-x}S_x$ series layered solids. J. Cryst. Growth **279**, 321–328 (2005)
26. A.M. Abd-Elnaiem, R.M. Hassan, H.R. Alamri, H.S. Assaedi, Comparative investigation of linear and nonlinear optical properties of As–70 at% Te thin films: infuence of Ga content. J. Mater. Sci. Mater. El. **31**, 13204–13218 (2020)
27. I. Isakov, H. Faber, A.D. Mottram, S. Das, M. Grell, A. Regoutz, R. Kilmurray, M.A. McLachlan, D.J. Payne, T.D. Anthopoulos, Quantum confinement and thickness-dependent electron transport in solution processed In_2O_3 transistors. Adv. Electron. Mater. **6**, 2000682 (2020)
28. G.B. Sakr, Optical and electrical properties of GaSe thin films. Mater. Sci. Eng. B **138**, 1–6 (2007)
29. S. Nakagomi, T. Sakai, K. Kikuchi, Y. Kokubun, β-Ga_2O_3/p-type 4H-SiC heterojunction diodes and applications to deep-UV photodiodes. Phys. Stat. Sol. A **216**, 1700796 (2019)
30. H. Belaid, M. Nouiri, A. Sayari, Z. Ben Ayadi, K. Djessas, L. El Mir, Modifications in electrical properties of ZnO:In/PS/Si (100) heterojunction by ZnO intermediate layer. Can. J. Phys. **93**, 1240–1245 (2015)
31. S.M. Sze, K.N. Kwok, *Physics of Semiconductor Devices* (Wiley, Hoboken, 2007)
32. A. Tataroglui, F.Z. Pur, The Richardson constant and barrier inhomogenity at Au/Si_3N_4/n-Si (MIS) Schottky diodes. Phys. Scr. **88**, 015801 (2013)
33. S. Duman, B. Gurbulak, M. Sata, Analysis of temperature dependent current-voltage characteristics of Sn/*p*-GaTe/In Schottky diode. Opt. Mater. **125**, 112138 (2022)
34. S.K. Mourya, G. Malik, B. Alisha, R.C. Kumar, The role of non-homogeneous barrier on the electrical performance of 15R–SiC Schottky diodes grown by in-situ RF sputtering. Mat. Sci. Semicon. Proc. **149**, 106855 (2022)
35. H. Kim, H.Y. Lee, B.J. Choi, Barrier inhomogeneity and leakage current transport mechanism in vertical Pt/Gd_2O_3/GaN Schottky diodes. Appl. Phys. **127**, 647 (2021)
36. S. Chand, J. Kumar, On the existence of a distribution of barrier heights in Pd_2Si/Si Schottky diodes. J. Appl. Phys. **80**, 288–294 (1996)
37. S. Chand, J. Kumar, Current-voltage characteristics and barrier parameters of Pd_2Si/p-Si(111) Schottky diodes in a wide temperature range, Semicon. Sci. Technol. **10**, 1680–1688 (1995)
38. S. Ruzgar, Y. Caglar, O. Polat, D. Sobola, M. Caglar, The influence of Fe substitution into photovoltaic performance of p-CuO/n-Si heterojunctions. J. Mater. Sci. Mater. Electron. **32**, 20755–20766 (2021)
39. S. Annathurai, S. Chidambaram, B. Baskaran, G.K.D.P. Venkatesan, Green synthesis and electrical properties of p-CuO/n-ZnO heterojunction diodes. J. Inorg. Organomet. Polym. Mater. **29**, 535–540 (2019)